

# BASIC AEROELASTIC STABILITY STUDIES OF HINGELESS ROTOR BLADES IN HOVER USING GEOMETRICALLY EXACT BEAM AND FINITE-STATE INFLOW

Mohammadreza Amoozgar,<sup>a</sup> Alessandro Croce,<sup>b</sup> Carlo E. D. Riboldi,<sup>b</sup> Lorenzo Trainelli,<sup>b</sup>

<sup>a</sup> Department of Aerospace Engineering, Amirkabir University of Technology, Tehran, Iran

<sup>b</sup> Department of Aerospace Science and Technology, Politecnico di Milano, Milano, Italy

Corresponding author: Mohammadreza Amoozgar [m.r.amoozgar@aut.ac.ir](mailto:m.r.amoozgar@aut.ac.ir)

## Abstract

An approach to aeroelastic stability analysis of hingeless rotor blades in hover is presented which combines a geometrically exact beam theory and a three-dimensional finite-state dynamic inflow theory, using the *Cp-Lambda* finite-element multibody code. The aeroelastic system is solved by an efficient numerical integration scheme, and the lead-lag damping is determined from the time response results. The method is validated by application to a two-bladed hingeless rotor without precone, and a remarkable agreement with reference results is observed, in dependence of the number of finite inflow states. Then, results are obtained with positive and negative precone angles, showing the effect of these variations on lead-lag stability.

## 1. INTRODUCTION

Hingeless rotors, such as those used in many rotary-wing aircraft applications, may suffer from dangerous instability problems due to aeroelastic coupling phenomena, especially with regards to the lightly damped in-plane lead-lag motion. The present paper illustrates a numerical study of the aeroelastic stability of a relatively simple hingeless blade in hover conditions making use of state-of-the-art modelling tools. These allow fine predictions of the behavior of the rotor system, which are first compared with the results obtained by other methods published in the literature and then presented for different cases as reference data for further studies and applications.

The aeroelastic stability analysis of rotorcraft blades is a multidisciplinary nonlinear problem in which a structural model of the blade must be strongly coupled with an unsteady aerodynamic load model. The structural model may use a moderate- or large-deflection blade model. Nowadays, given the progress in computational methods, the large-deflection approach, with no restrictions on displacements and rotations, is favored by many analysts. The structural modelling fidelity is crucial in aeroelastic analysis, as shown by the results in Refs. 1–3, where the dependence of the aeroelastic behavior on the beam geometry and cross-sectional elastic couplings is discussed.

The aerodynamic model may consider classical two-dimensional aerodynamics, vortex theory, and dynamic inflow theory. While the former is often unable to effectively model the three-dimensional effects which significantly impact the rotor aeroelastic behavior, the latter two approaches are often employed in view of accurate results. However, the computational cost of vortex theories which are originally developed from propeller analysis, is often high.<sup>[4,5]</sup> A convenient alternative is represented by the coupling of the two-dimensional thin airfoil theory with finite-state dynamic inflow models. The best known representative of the latter was developed in Ref. 6. This theory has been used extensively in aeroelastic analysis of hingeless rotors blades.<sup>[7–9]</sup> Indeed, Ref. 9 presents a recent study considering the inflow modelling effects on the aeroelastic stability of hingeless and bearingless rotors by using a large-deflection beam theory. The study shows that, at low advance ratios, the predicted damping values are affected by the type of wake used in the simulations, while this phenomenon fades out at higher advance ratios.

The present study employs a multibody system dynamic approach. This is widely used as a fundamental design tool in many engineering disciplines, such as aerospace, automotive and wind energy. Within this approach, any arbitrarily complex-topology mechanism can be modeled by combining different flexible or rigid elements with the use of several mechanical joints (such as revolutes, prismatic, planar, etc.), actuator elements, force fields, control systems, etc. Therefore, the

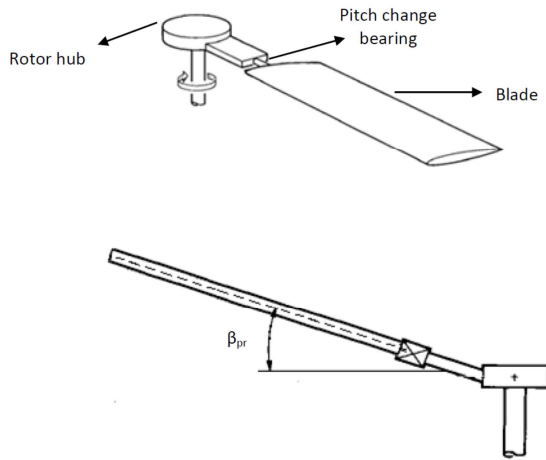


Figure 1: Schematic of a hingeless rotor blade with precone angle.

simple model considered in this study can be easily embedded within a complex assembly representing a complete rotor, or even a complete rotorcraft vehicle. Recent examples of applications of this approach to the high-fidelity dynamic analysis of helicopter rotor assemblies are given by Refs. 10–11, while Refs. 12–13 report on the modelling and simulation of complete rotorcraft vehicles.

## 2. FORMULATION

In this study a hingeless rotor blade with precone is considered, as shown in Figure 1. This system was implemented in the advanced aero-servo-elastic *Cp-Lambda* simulation tool. This is a nonlinear finite-element (FE) multibody code extensively employed in the analysis of rotorcraft and wind-energy industrial systems.<sup>[10–17]</sup>

*Cp-Lambda* provides a large library of structural elements such as rigid bodies, composite-capable beams and shells, cables, and joint models, which can be equipped with concentrated stiffness and damping, backlash, free-play and friction. In particular, the elastic beam model is based on a geometrically exact approach which allows arbitrarily large nonlinear displacements and rotations, as well as a complete cross-section inertial and stiffness coupling.

Lagrange multipliers enforce the kinematical constraints in an optimized index-3 DAE (differential-algebraic equations) fashion.<sup>[18]</sup> Among the force fields that can be associated to body

elements, aerodynamic forces are modelled according to a lifting-line approach based on 2D aerofoil coefficients. Inflow elements can be associated to rotors, such as the blade-element momentum (BEM) model based on the annular stream-tube theory with wake swirl, or the Peters–He finite-state wake model.<sup>[6]</sup> For numerical robustness, the *Cp-Lambda* solver employs time marching schemes that enforce a tuneable algorithmic energy dissipation, thus providing a built-in filter for unresolved high frequencies arising from FE discretization.<sup>[19]</sup>

A second modelling approach is also considered, by adopting a geometrically exact fully intrinsic beam formulation. This considers the equations of motion for the dynamics of beams written in intrinsic form, *i.e.* avoiding the presence of displacement and rotation variables.<sup>[20]</sup> This approach was used in Ref. 21, using a discretization based on 8 sampling points along the blade span and a quasi-steady Greenberg aerodynamic theory.<sup>[22]</sup>

## 3. NUMERICAL STUDIES

The system considered is a simple isolated, two-bladed hingeless rotor with untwisted, isotropic blades. Each blade has been modeled as a uniform beam with center of mass axis, tension axis, and aerodynamic center axis coincident with the elastic axis. The rotor characteristics and the blade material and aerodynamic properties are listed in Table 1 (see Ref. 4 for further details).

The discretization makes use of using 10, 3<sup>rd</sup> order elements, with a lifting line with 100 air-stations along the blade span, and a Peters-He inflow with a user-specified number of states, ranging from 1 (uniform inflow) to 15.

First the validity of the developed aeroelastic model was assessed by comparison with results provided in Ref. 4. There, a quasi-steady two-dimensional (QS-2D) aerodynamic model and a more complex three-dimensional vortex-lattice method (VLM) have been applied to the same structural blade in the context of a large-deflection beam theory. The steady-state blade tip deflections in the flap and lead-lag directions have been computed for a null precone angle, as a function of blade pitch. These resulted in two clearly distinct pairs of curves, shown in Figures 2 and 3, together with the results here obtained spanning 5 possible values of the Peters-He number of states (NOS), ranging from 1 to 15. Also, the results presented in Ref. 21 are included.

Table 1: Rotor characteristics.

|  |                 |         |
|--|-----------------|---------|
| Rotor solidity   | $\sigma$        | 0.06189 |
| Blade aspect ratio   | $c/R$           | 0.09722 |
| Non-dimensional fundamental lead-lag natural blade circular frequency  | $\omega_v$      | 1.30    |
| Non-dimensional fundamental flap natural blade circular frequency      | $\omega_w$      | 1.14    |
| Non-dimensional fundamental torsion natural blade circular frequency   | $\omega_\phi$   | 3.00    |
| Ratio of blade cross-section polar radius of gyration and blade radius | $k_m/R$         | 0.02778 |
| Ratio of principal mass radii of gyration                              | $k_{m1}/k_{m2}$ | 0       |
| Lock number  | $\gamma$        | 6.308   |
| Blade airfoil lift-curve slope   | $C_{l_\alpha}$  | $2\pi$  |
| Blade airfoil passive drag coefficient                                 | $C_{d_0}$       | 0.01    |

It can be seen that, for both the flap and lead-lag deflections, using a quasi-steady two-dimensional model leads to similar results. On the other hand, a clear trend towards convergence is observed when changing the Peters-He number of states from 1 to 15. The convergence values do not fit the VLM results. However, these results are assumed sufficient to validate the static behavior of the developed model.

For the same case, the dynamic behavior is appraised by comparing the normalized lead-lag damping values obtained by the different methods. The lead-lag damping has been obtained by inspection of the time response of the system when perturbed from the steady hover conditions. Here, the VLM results refer to the two modes exhibited by the two-blade rotor, namely the collective and differential modes, as an effect of the unsteady inflow generated by shed vorticity. However, both modes appear at the same frequency.

Figure 4 shows the comparison with the methods presented here. The damping curves are shown starting from the origin and rising as the pitch

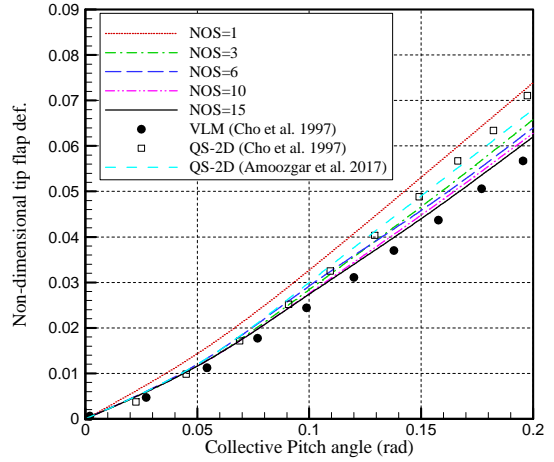


Figure 2: Equilibrium tip flap deflection at different collective pitch angles and various numbers of inflow in the case of null precone.

increases. Here again, the quasi-steady two-dimensional approaches lead to similar results, distinctly far away from those obtained by the VLM and the Peters-He results with  $NOS > 1$ , which appear in close agreement. Note that the quasi-steady two-dimensional methods result in higher values than that of the unsteady three-dimensional methods. Also, as seen in the previous figures, the differences between the values obtained by varying the number of inflow states increase, albeit slightly, as the pitch increases.

The next study concerns the same isotropic blade set at a positive precone angle of 0.05 rad, *i.e.* in

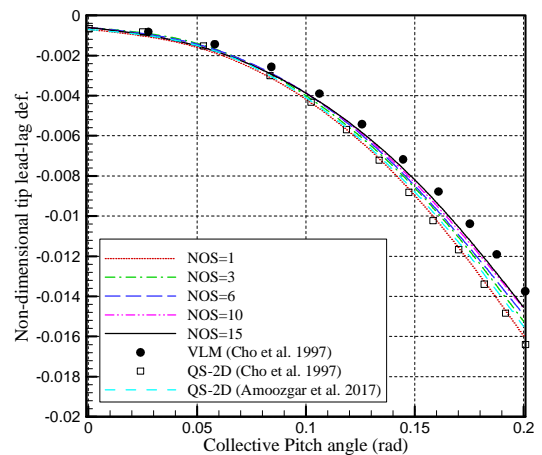


Figure 3: Equilibrium tip lead-lag deflection at different collective pitch angles and various numbers of inflow states in the case of null precone.

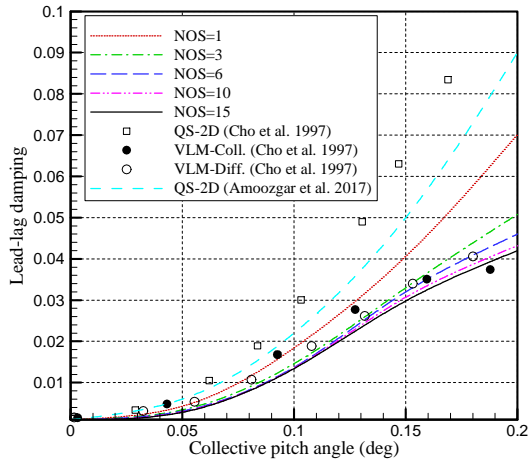


Figure 4: Aeroelastic lead-lag damping at different collective pitch angles and various numbers of inflow states in the case of null precone.

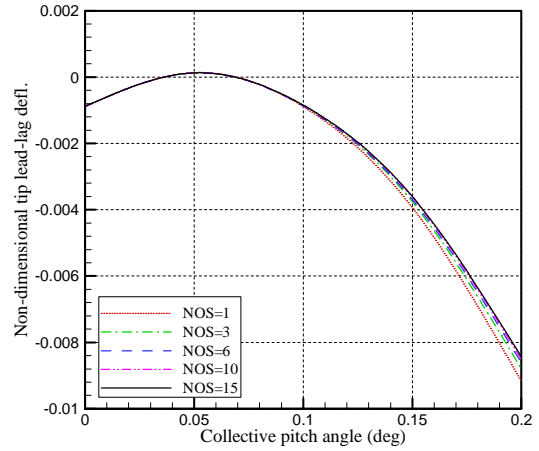


Figure 6: Equilibrium tip lead-lag deflection at different collective pitch angles and various numbers of inflow in the case of positive 0.05 rad precone.

the upward flap direction. Figures 5 and 6 show the tip steady-state flap and lead-lag deflections at varying pitch angles and for different numbers of inflow states. By comparing these plots with the results of the case without precone angle (Figures 2 and 3), it is deduced that the positive precone angle decreases both the flap and lead-lag deflections. As before, a clear trend towards convergence is observed when increasing the Peters-He number of states from 1 to 15.

Figure 7 shows the normalized lead-lag damping values found in this case. It is apparent that the

effect of the positive precone angle changes the behavior of the damping, generating a region of instability. In fact, now at null pitch angle the damping is positive and increasing the pitch angle from the damping decreases, vanishing in the vicinity of a pitch angle value of 0.025 rad. Further increases in pitch lead to reach a minimum damping at about 0.050 rad, after which the stability boundary is attained again close to 0.080 rad. A pitch increase from this point induces a positive stability, with monotonic growth of the damping value. It can be noted that, for this case, all curves essentially predict the same stability boundary.

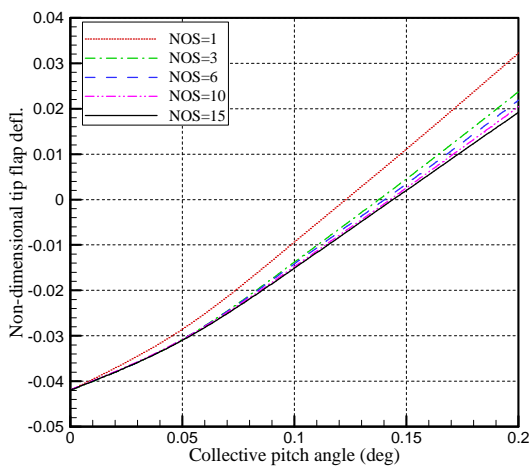


Figure 5: Equilibrium tip flap deflection at different collective pitch angles and various numbers of inflow in the case of positive 0.05 rad precone.

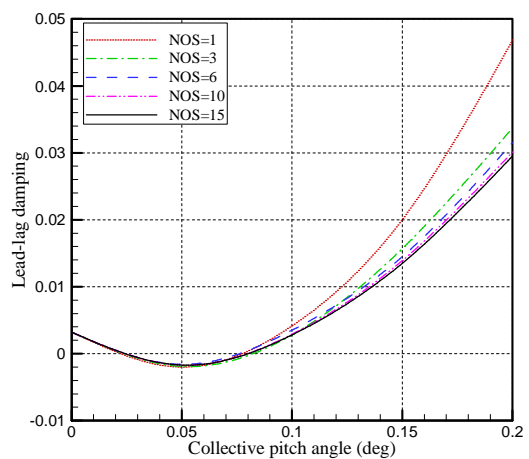


Figure 7: Aeroelastic lead-lag damping at different collective pitch angles and various numbers of inflow states in the case of positive 0.05 rad precone.

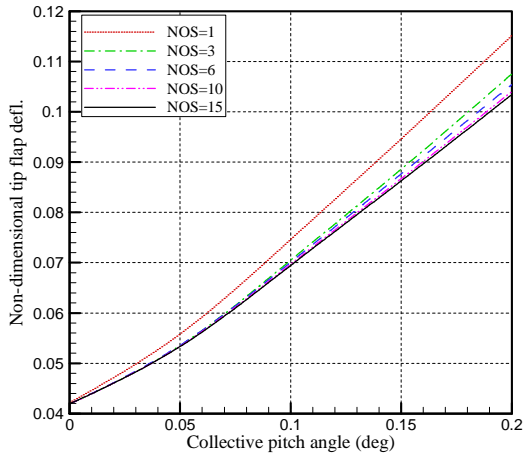


Figure 8: Equilibrium tip flap deflection at different collective pitch angles and various number of inflow in the case of negative 0.05 rad precone.

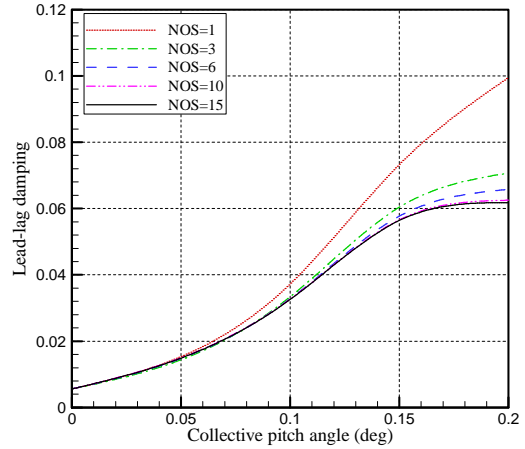


Figure 10: Aeroelastic lead-lag damping at different collective pitch angles and various number of wake states in the case of negative 0.05 rad precone.

A different behavior is observed when the same isotropic blade set at a negative precone angle of 0.05 rad, *i.e.* in the downward flap direction. Figures 8 and 9 show the tip steady-state flap and lead-lag deflections at varying pitch angles and for different numbers of inflow states. Also in this case, a clear trend towards convergence is observed when increasing the Peters-He number of states. However, the negative precone angle increases both the flap and lead-lag deflections, compared to the null precone case.

Similarly, the damping values are higher and therefore the system is more stable than the case of

null or positive precone angle, as shown in Figure 10. Indeed, the damping at zero pitch is positive and steadily grows as pitch increases. Again, relatively low values of the number of inflow states, such as 3 or 6, is sufficient to predict the damping with a reasonable accuracy up to a pitch of 0.10 rad or higher.

In order to further illustrate the changes in stability generated by pre-coning, a number of time histories for the tip displacements resulting from a perturbation in the steady-state hover conditions are included next.

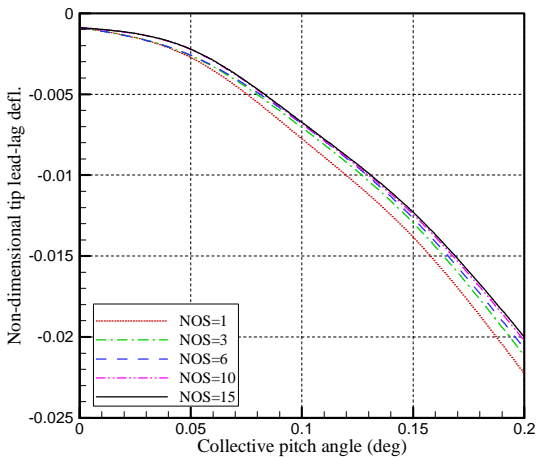


Figure 9: Equilibrium tip lead-lag deflection at different collective pitch angles and various number of inflow in the case of negative 0.05 rad precone.

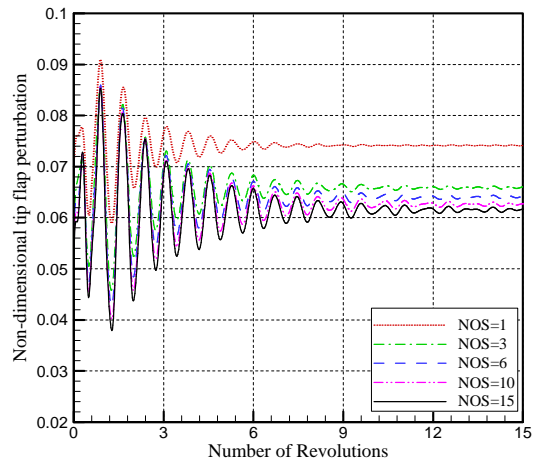


Figure 11: Stable tip flap deflection time histories at 0.20 rad pitch and various number of inflow states in the case of null precone.

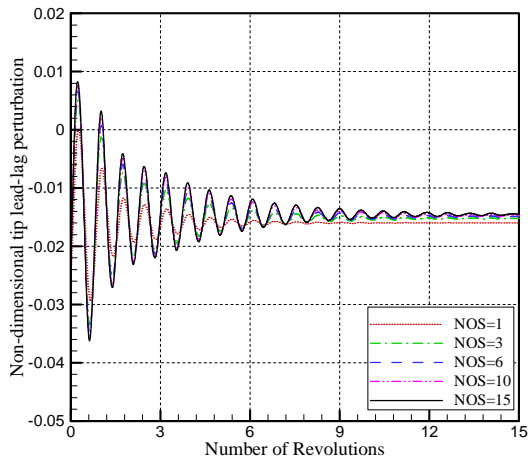


Figure 12: Stable tip lead-lag deflection time histories at 0.20 rad pitch and various number of inflow states in the case of null precone.

First, for the case of a null precone, Figures 11 and 12 show the blade tip flap and lead-lag displacements in time at a pitch of 0.20 rad, *i.e.* in a highly stable condition. The curves corresponding to the full range of the number of inflow states are displayed. The asymptotic values, corresponding to those shown in Figures 5 and 6, are apparent. Also, the overestimation of the damping for NOS = 1 (higher than 0.04) with respect to the cases of higher NOS (all about 0.03) clearly appears.

Second, the case of a positive 0.05 rad precone is considered. Figures 13 and 14 show the blade tip flap and lead-lag displacements in time at two

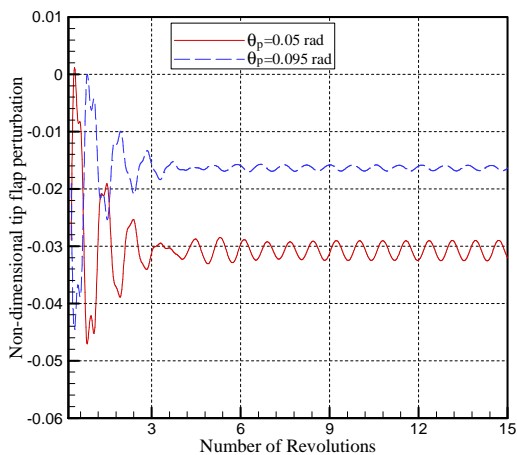


Figure 13: Tip flap deflection time histories at 0.05 rad (red, unstable) and 0.095 rad (blue, stable) for 15 inflow states in the case of positive 0.05 rad precone.

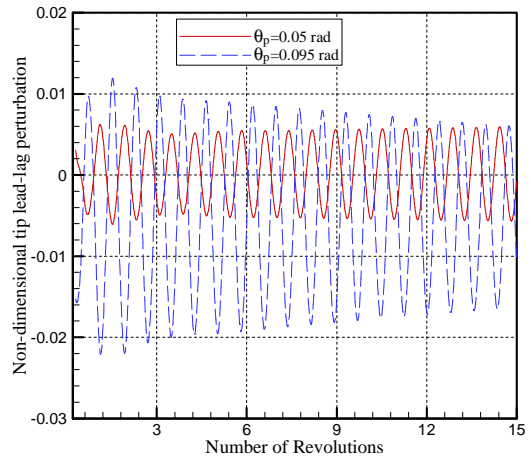


Figure 14: Tip lead-lag deflection time histories at 0.05 rad (red, unstable) and 0.095 rad (blue, stable) for 15 inflow states in the case of positive 0.05 rad precone.

different pitch values, one in the unstable region and one in the stable region, characterized by equal absolute value of the damping coefficient. These are found at 0.05 rad and 0.095 rad, respectively. The initial perturbation (a tip dead load) has the same intensity in the two cases, but being applied on the same material axis, results in a different loading conditions due to the different collective pitch. Only the results for NOS = 15 are shown. Although the absolute value of the damping is small, the graphs show a fairly clear divergent and convergent behavior, respectively.

#### 4. CONCLUDING REMARKS

In this paper, the aeroelastic stability and response of an isolated hingeless rotor in hover has been investigated. A simple blade model, implemented within a state-of-the-art aero-servo-elastic simulation tool based on a consolidated and numerically efficient finite-element multibody dynamics formulation, has been considered, looking in particular at equilibrium tip deflections and at lead-lag modal damping values, as retrieved from the analysis of perturbed time responses. The model allows a user-defined number of states for the Peters-He finite-state wake model and the study reveals that the solution can be considered converged when using 15 states.

The results relative to a null precone case appear very well correlated with three methods present in the known literature, suggesting that in this case a

relatively low number of inflow states (between 3 and 10) is sufficient for practical purposes.

The effect of positive and negative precone has been investigated, showing the destabilizing effect of the former and the stabilizing effect of the latter. Indeed, in the case of positive precone, a region of lead-lag instability appears. Again, a relatively low number of inflow states is sufficient to capture the stability boundary.

The present study is intended as a preparatory step in view of the analysis of more complex problems of industrial relevance, related to the aeroelastic design and verification of hingeless and bearingless rotors.

## 5. REFERENCES

- [1] Fulton MV, Hodges DH. Aeroelastic stability of composite hingeless rotor blades in hover—Part I: Theory. *Mathematical and Computer Modelling*, Vol. 18, No. 3/4, pp. 1–17, 1993.
- [2] Fulton MV, Hodges DH. Aeroelastic stability of composite hingeless rotor blades in hover—Part II: Results. *Mathematical and Computer Modelling*, Vol. 18, No. 3/4, pp. 19–35, 1993.
- [3] Cho MH, Lee I. Aeroelastic stability of hingeless rotor blade in hover using large deflection theory. *AIAA Journal*, Vol. 32, No. 7, pp. 1472–1477, 1994.
- [4] Cho MH, Jeon SM, Woo SH, Lee I. Refined aeroelastic analysis of hingeless rotor blades in hover. *Journal of Aircraft*, Vol. 34, No. 3, pp. 408–415, 1997.
- [5] Shahverdi H, Nobari AS, Behbahani-Nejad M, Haddadpour H. Aeroelastic analysis of helicopter rotor blade in hover using an efficient reduced-order aerodynamic model. *Journal of Fluids and Structures*, Vol. 25, pp. 1243–1257, 2009.
- [6] Peters DA, He CJ. Finite state induced flow models. Part II: Three-dimensional rotor disk. *Journal of Aircraft*, Vol. 32, No. 2, pp. 323–333, 1995.
- [7] Tang D, Dowell EH. Nonlinear rotor aeroelastic analysis with stall and advanced wake dynamics. *Journal of Aircraft*, Vol. 34, No. 5, pp. 679–687, 1997.
- [8] Shang X, Hodges DH, Peters DA. Aeroelastic Stability of Composite Hingeless Rotors in Hover with Finite-State Unsteady Aerodynamics. *Journal of the American Helicopter Society*, Vol. 44, No. 3, pp. 206–221, 1999.
- [9] Jeong MS, Lee I, Yoo SJ, Yun CY, Kim DK. Wake effects on aeroelastic stability of hingeless and bearingless rotors. *Journal of Aircraft*, Vol. 50, No. 6, pp. 1938–1943, 2013.
- [10] Croce A, Possamai R, Savorani A, Trainelli L. Modelling and Characterization of a Novel Gimbal Two-Blade Helicopter Rotor. Proc. 40<sup>th</sup> European Rotorcraft Forum (ERF2014), Southampton, UK, paper no. 079, 2014.
- [11] Croce A, Possamai R, Trainelli L. Dynamic Properties of Some Gimbal and Teetering Two-Blade Helicopter Rotor Heads. Proc. 40<sup>th</sup> European Rotorcraft Forum (ERF2014), Southampton, UK, paper no. 080, 2014.
- [12] Trainelli L, Croce A, Riboldi CED, Possamai R. Trimming a High-Fidelity Multibody Helicopter Model for Performance and Control Analysis. Proc. 41<sup>st</sup> European Rotorcraft Forum (ERF 2015), Munich, Germany, paper no. 120, 2015.
- [13] Riboldi CED, Croce A, Trainelli L, Capocchiano C, Pinato D. A Model-Based Design Framework for Rotorcraft Trim Control Laws. Proc. 43<sup>rd</sup> European Rotorcraft Forum (ERF 2017), Milano, Italy, paper no. 733, 2017.
- [14] Bottasso CL, Trainelli L, Abdel-Nour P, Labò G. Tilt Rotor Analysis and Design Using Finite-Element Multibody Dynamics Proc. 28<sup>th</sup> European Rotorcraft Forum (ERF 2002), Bristol, UK, 2002.
- [15] Bottasso CL, Croce A, Leonello D, Riviello L. Steering of Flexible Multibody Models with Application to the Simulation of Maneuvering Flight. Proc. 4<sup>th</sup> European Congress on Computational Methods in Applied Sciences and Engineering (ECCOMAS 2004), Jyväskylä, Finland, 2004.
- [16] Bottasso CL, Riviello L. Trim of rotorcraft multibody models using a neural-augmented model-predictive auto-pilot. *Multibody System Dynamics*, Vol. 18, No. 3, pp 299–321, 2007.
- [17] Bottasso CL, Croce A, Savini B, Sirchi W, Trainelli L. Aeroelastic Modeling and Control of

Wind Turbine Generators Using Finite Element Multibody Procedures. *Multibody System Dynamics*, Vol. 16, No. 3, pp. 291–308, 2006.

- [18] Bottasso CL, Dopico D, Trainelli L. On the Optimal Scaling of Index Three DAEs in Multibody Dynamics. *Multibody System Dynamics*, Vol. 19, No. 1/2, pp. 3–20, 2008.
- [19] Bauchau OA, Bottasso CL, Trainelli L. Robust Integration Schemes for Flexible Multibody Systems. *Computer Methods in Applied Mechanics and Engineering*, Vol. 192, No. 3/4, pp. 395–420, 2003.
- [20] Borri M, Mantegazza, P. Some Contributions on Structural and Dynamic Modeling of Helicopter Rotor Blades. *Aerotecnica Missili e Spazio*, Vol. 64, No. 9, pp. 143–154, 1985.
- [21] Amoozgar MR, Shahverdi H, Nobari AS. Aeroelastic stability of hingeless rotor blades in hover using fully intrinsic equations. *AIAA Journal*, 2017 (published online). doi: <http://dx.doi.org/10.2514/1.J055079>.
- [22] Greenberg JM. Airfoil in sinusoidal motion in pulsating stream. NACA Technical Report TN 1326, 1947.